Atmos. Chem. Phys. Discuss., 9, 18621–18657, 2009
www.atmos-chem-phys-discuss.net/9/18621/2009/

Atmospheric Chemistry and Physics Discussions

This discussion paper is/has been under review for the journal *Atmospheric Chemistry and Physics (ACP)*. Please refer to the corresponding final paper in *ACP* if available.

Regional-scale correlation between CO_2 fire emissions, burned areas, and mid-tropospheric CO_2 daily variations over southern Africa

A. Chédin[1], N. A. Scott[1], P. Ciais[2], C. Rio[3], F. Hourdin[3], C. Crevoisier[1], and R. Armante[1]

[1]Laboratoire de Météorologie Dynamique, IPSL, Ecole Polytechnique, 91128 Palaiseau, France
[2]LSCE, UMR CEA-CNRS, CE, L'Orme des Merisiers, Gif-sur-Yvette, France
[3]Laboratoire de Météorologie Dynamique, IPSL, Université P. et M. Curie, 75252 Paris, France

Received: 16 July 2009 – Accepted: 21 August 2009 – Published: 10 September 2009

Correspondence to: A. Chédin (chedin@lmd.polytechnique.fr)

Published by Copernicus Publications on behalf of the European Geosciences Union.

Abstract

Monthly mean mid-tropospheric CO_2 columns are retrieved from evening and morning observations of NOAA-10 satellite over the tropics during the period 1987–1991. We find that the difference between evening and morning CO_2 columns (hereafter referred to as Daily Tropospheric Excess – DTE) increases by up to a few ppm over regions affected by fires. A high positive correlation (R^2~0.8) is found between annual DTE and CO_2 emissions derived from burned area (Global Fire Emission Database – GFEDv2) across 10 regions with contrasted vegetation cover in southern Africa. Seasonal variability comparison between DTE and GFEDv2 also shows a good general agreement. Only two regions south of 10° S, show a seasonal increase of DTE starting earlier and rising up more rapidly than seen in two burned area products: GFEDv2 and L3JRC, the latter established by the Joint Research Center. The phase of the L3JRC dataset is however closer to DTE observations. This misfit could come from limitations in current burned area detection algorithms (difficulty in detecting small fires). 3-D simulations of the DTE signal by the LMDz General Circulation Model, in which a pyro-thermal plume model is activated, confirm the observations. A large fraction of fire products are directly injected in the mid-troposphere, well above the boundary layer. This rapid uplift of CO_2, combined with atmospheric transport patterns in southern Africa during the dry season, characterized by a fluctuating continental gyre, produces a daily DTE signal mainly positive above the source region and either positive or negative outside of the source region. On a monthly mean, this results in a persistent DTE signal above the source region of an order of 1 ppm, while the impact of large-scale advection vanishes. We conclude that the DTE signal is a quantitative proxy of fire emission spatial patterns, in particular before the ATSR or MODIS observation periods when better quality fire count and burned area data became available, and can also bring a constraint in the analysis of their present results.

1 Introduction

Biomass burning is a large source of atmospheric CO_2, CO, aerosols and chemically important trace gases and a major component of the carbon cycle and Earth climate system. Average annual carbon emissions from fires are around 2.5 Pg C yr^{-1} with African emissions accounting for 50% of the total, equally distributed over both hemispheres (van der Werf et al., 2006). However, estimates of CO_2 emissions from fires still suffer from large uncertainties. In particular, the relationship between emissions, climate and human activities is still uncertain. This is particularly true for tropical fires which are suspected to cause most of the year-to-year variability in the growth rate of atmospheric CO_2 and other key species (e.g. Langenfelds et al., 2002; van der Werf et al., 2004). Within the tropics, savanna fires alone contribute roughly 20% of the emissions (Andreae, 1996). This large source of CO_2 associated to savanna fires is highly seasonal and it is offset during the wet season by CO_2 uptake associated to re-growth. The extent to which savanna ecosystems are today carbon neutral with respect to fires is unknown, although there is some evidence that savanna fires have increased during the 20th century in response to rising population (Mouillot and Field, 2005; Crutzen and Zimmermann, 1991; van Aardenne et al., 2001).

Numerical simulations suggest a moderate effect of biomass burning on the CO_2 seasonal cycle, as measured at the global network of marine stations (Wittenberg et al., 1998; van der Werf et al., 2004) but a large impact on the interannual growth rate variability (Langenfelds et al., 2002; van der Werf et al.; 2004, Patra et al., 2005). However, the scarcity of surface stations implies that the tropical carbon balance remains largely un-constrained. Moreover, interannual variations of reactive species such as CO, CH_4, H_2 have been observed to closely correlate with those of CO_2 (Langenfelds et al., 2002). This suggests that climate induced fluctuations of fire emissions play a major role in the variability of tropical and global atmospheric chemistry. In that context, any knowledge of fire emissions derived from CO_2 atmospheric observations has also great potential to deliver a better understanding of the cycles of reactive species.

ACPD
9, 18621–18657, 2009

The amount of CO_2 released to the atmosphere by fire is generally estimated as the product of burned area by fuel loads and combustion completeness. Burned area is considered to be the most uncertain parameter in emission estimates on a global scale (Mouillot and Field, 2005; Palacios-Orueta et al., 2005; van der Werf et al., 2006). Burned area is usually derived from satellite observations (Barbosa et al., 1999; Schultz, 2002; Duncan et al., 2003; Ito and Penner, 2004; Kasischke and Penner, 2004; Hoelzemann et al., 2004; van der Werf et al., 2006; Giglio et al., 2006a, b; Tansey et al., 2008a), and used as an input of fire modules in vegetation models (van der Werf et al., 2003, 2004; Randerson et al., 2005).

Maps of fire emissions derived from satellite observations of fire hot spots (counts) or burned scars remain highly uncertain. Moreover, the burned-area-based approach to estimate emissions is limited to the time period of adequate satellite observations, typically the past 10 years. This hampers diagnostic of the long-term evolution of fires, as well as projection of future trends and understanding of fire/climate relationships.

Recently, global observations of upper-air CO_2 have become available from space-borne infrared sounders, providing information on the variation of its concentration (seasonal, interannual, trend), in the tropical mid-troposphere. Monthly mean CO_2 columns have been retrieved from evening (19:30 LST) and morning (07:30 LST) observations of the TOVS instruments flying onboard the NOAA polar satellites (Chédin et al., 2002, 2003a). A strong correlation (R^2~0.8) was found between CO_2 emissions from the Global Fire Emission Dataset, version 2 (GFEDv2; Randerson et al., 2006) and the difference between evening minus morning column CO_2 from TOVS, hereafter called Daily Tropospheric Excess (DTE). It was shown that the DTE exhibits continental-scale spatio-temporal patterns that are in good agreement with burned-area based CO_2 emissions over most of the tropical regions affected by fires (Chédin et al., 2005, 2008). It was also shown that DTE displays interannual variability which correlates well with ENSO, as for fire emissions themselves (Chédin et al., 2008). The DTE signal could thus be used as a proxy of CO_2 emissions to reconstruct fire emission before the ATSR and MODIS era. Burned area data could also benefit from constraints

brought by DTE observations derivable from the new generation sounder Infrared Atmospheric Sounder Interferometer (IASI) operational since 2006 (Chédin et al., 2003b).

The correlation between DTE and fire emissions in tropical regions seems to be related to the strong diurnal cycle affecting fires (Giglio, 2007 and references herein). A possible mechanism for CO_2 concentration being higher in the afternoon than in the morning is that hot convective fire plumes inject emissions directly into the troposphere during the afternoon peak of fire activity, seen by the satellite at 19:30 LST, and then diluted by large-scale atmospheric transport before the next satellite pass at 07:30 LST. Even if no direct observations have confirmed the existence of such a mechanism over southern Africa, several studies bring some credibility to it. In particular, Rio et al. (2009) simulate a DTE signal of an order of 1 ppm over southern Africa by including a scheme for pyro-convection, the "pyro-thermal plume model", in the General Circulation Model LMDz (Hourdin et al., 2006), and Freitas et al. (2007), using a regional model including the representation of the transport by convective plumes generated by fires, simulate injection heights reaching 7 km over southern Africa. Chédin et al. (2008) found high positive correlations between DTE and tropical fire emissions at continental scale in Africa but they did not investigate correlations at regional scale, a relevant scale at which vegetation cover and fire susceptibility relationships might become more homogeneous.

We present in this paper an in-depth regional-scale analysis of the DTE distribution inferred from NOAA-10 over southern hemisphere Africa from 1987–1991. Comparisons are made between DTE and two fire CO_2-emission datasets: the Global Fire Emission Dataset, version 2 (GFEDv2; Randerson et al., 2006) covering the period 1997–2004, and the global burnt areas dataset of the Joint Research Center (L3JRC) (Tansey et al., 2008a) covering the period 2000–2007. Results from simulations by LMDz including the pyro-thermal plume model (Rio et al., 2009) are further analysed here to investigate the credibility of the mechanisms suggested by the observations.

In the following, we first describe the methodology used (Sect. 2). Then, we discuss comparisons between the DTE and fire emission datasets (Sect. 3). Results from DTE

simulations by the LMDz model are presented in Sect. 4, and conclusions are drawn in Sect. 5.

2 Methodology

2.1 The study regions

Africa represents some 50% of the total fire emissions – roughly evenly distributed into both hemispheres. It is probably the continent for which fire activity has been studied most in depth. Therefore, there are different fire emission related datasets (emissions, burned areas, etc.). Due to a strong and rather long dust aerosol season, partly overlapping with the dry fire season, northern Africa (NAF) is less suitable to a regional-scale study of CO_2 from space observations than is southern Africa (SAF). As reported by van der Werf et al. (2006), if emissions from SAF ($\sim$580 Tg C yr^{-1}) are somewhat smaller than emissions from NAF ($\sim$630 Tg C yr^{-1}), the average fuel consumption appears to be higher in SAF. This is because of more woodland fires in SAF, against savannas fires in NAF.

Following Hoelzemann (2006), SAF has been divided into 10 sub-regions with different vegetation characteristics (Mayaux et al., 2004; DeFries et al., 1998). This is illustrated in Fig. 1. Region 1 is dominated by tropical forests; region 2 by grasslands with some forests, woodlands and shrublands; regions 3 and 5 by closed deciduous forests and mosaic forest/savanna. Woodlands and shrublands dominate regions 4 and 6. Grasslands dominate region 7. Both woodlands and grasslands dominate region 8. Region 9 is a mix of woodlands, croplands, grasslands and forests and region 10 of grasslands, shrublands and mosaic forest/savanna. Additionally, we define two larger regions, called ASs (south of 14° S) and ASn (north of 14° S), covering the southern and the northern parts of southern Africa, respectively (Table 1). In both GFEDv2 (CO_2 emissions) and L3JRC (burnt areas) datasets, the highest relative contributors to SAF emissions are regions 3, 5, 4 and 6 – in this order – i.e. the four regions with higher

ACPD
9, 18621–18657, 2009

woody vegetation coverage.

2.2 Observed diurnal anomaly of CO_2 in the troposphere

Flying aboard the National Oceanic and Atmospheric Administration (NOAA) polar meteorological satellites since 1978 (Smith et al., 1979), the TOVS instrument consists of the High resolution Infrared Radiation Sounder (HIRS-2), the Microwave Sounding Unit (MSU) and the Stratospheric Sounding Unit (SSU). In the 15 µm and 4.3 µm spectral bands, HIRS-2 radiances mostly depend on the temperature of the atmosphere but also, although weakly (Chédin et al., 2002), on the CO_2 concentration. The MSU observations are also sensitive to temperature, but are insensitive to CO_2. Combining HIRS-2 and MSU allows separating the two signals. The approach developed by Chédin et al. (2003a, 2005, 2008) to retrieve CO_2 is based upon a non-linear regression inverse radiative transfer model based on the Multi-Layer Perceptron (Rumelhart et al., 1986) and was applied to NOAA-10 observations.

The retrieved CO_2 columns are weighted to the tropical mid-troposphere with a peak sensitivity at ~300 hPa, half the peak sensitivity at ~120 and ~600 hPa, and no sensitivity to the surface (see Fig. 1 in Chédin et al., 2003a). Mid-tropospheric CO_2 columns were retrieved from NOAA-10 observations at 07:30 LST (daytime) and 19:30 LST (nighttime), between January 1987 and August 1991, in the tropical zone (30° N–30° S) where most of the biomass burning emissions are located. This period is marked by the end of the 1986–1987 El Nino, followed by a strong La Nina episode in 1988–1989, and by the beginning of a weak El Nino at the end of 1990 (see discussion in Chédin et al., 2005, 2008).

In the present study, individual daily CO_2 column retrievals are produced at a spatial resolution of 1°×1°. Morning and evening CO_2 retrievals are then collocated: within a 1°×1° grid box, a morning daily CO_2 retrieval is retained only if an evening retrieval is found during the same day. If this collocation criterion is met, the difference between the evening and the morning CO_2 retrievals is formed, which defines one item of the 1°×1° DTE data set. Oppositely, if the collocation is not met, the CO_2 retrieval is rejected.

These individual DTE items are then averaged temporally over a month. Areas with no data reflect the presence of a persistent cloudiness. As shown in Chédin et al. (2008), the DTE monthly mean accuracy is of the order of 0.4–0.5 ppm. This relatively good accuracy is due to the nature of this variable. Being differential, it is almost insensitive to instrumental or platform (drift) problems and show a low sensitivity to the two main potential sources of contamination that are ozone and aerosols. Moreover, the burning season in SAF is characterized by rather low levels of such contaminants (Ziemke et al., 2006; Bryant et al., 2007).

As shown by Chédin et al. (2008), the striking DTE property is the existence of regional maxima of several ppm over areas affected by fires. This is illustrated for SAF by Fig. 2 which displays four year averaged seasonal DTE maps. The DTE patterns shown by this figure are in agreement with the fire counts analysis of Cahoon et al. (1992) who described the west-to-east displacement of fires between March and November, due to drier conditions spreading from Namibia to the East. In May, biomass burning is widespread into SAF western and interior regions. In June, it peaks over the southern part of the Democratic Republic of Congo. From July to October, biomass burning spreads to the East and wanes in western and interior regions. Finally, from November to December, fires persist along the eastern coast of SAF (Kenya, Tanzania) and cease in December. At continental-scale, the seasonal variability of DTE was already characterized to be in good agreement (R^2~0.8) with GFEDv2 fire CO_2 emissions. Characteristic inter-annual changes in fire activity during the transition from El Niño to La Niña were also found to be in agreement between the DTE and GFEDv2 products, despite the different El Niño-to-La Niña transitions covered by each dataset.

2.3 Fire emission related products

The question of whether or not DTE is a proxy of fire activity at regional scale can be addressed by comparing it to two datasets established specifically to quantify fire emissions: 1) the GFEDv2 emission dataset based upon MODIS burned area data encapsulated into the Carnegie Ames Stanford Approach (CASA) biogeochemical model

(Potter et al., 1993; Randerson et al., 1996), and 2) the L3JRC-global burned areas dataset based upon SPOT-Vegetation burned areas (Tansey et al., 2008a). The GFEDv2 dataset covers the period 1997–2004 at a resolution of 1°×1°. The L3JRC dataset covers the period 2000–2007 (March 2007) at a spatial resolution of 1 km. Here, we used data averaged at 1°×1°. Lehsten et al. (2009) corrected the L3JRC burned area estimates for the bias introduced by low-resolution observations, and accounting for the standard deviation observed around the best-fit line when compared to a number of Landsat TM images. These improvements, not included in the L3JRC dataset used here, do not affect the seasonal cycle comparisons. Obviously, comparison with DTE observed during the period 1987–1991 is limited by the different time span of observations. However over SAF, interannual changes and trends remain relatively small compared to yearly mean values and seasonal amplitudes (van der Werf et al., 2008).

3 Comparisons of DTE with fire related products

Comparisons only include grid points of 1° by 1° in which there is a fire signal. This is defined by CO_2 emissions higher than 1 g CO_2 m^{-2} in GFEDv2 and burned fractions greater than 0.002 in L3JRC. Similarly, grid points with DTE values within the interval ±0.3 ppm (see Sect. 4) are discarded.

3.1 Annual means: a quantitative relationship at regional scale

Figure 3 compares DTE in ppm, with GFEDv2 emissions in g CO_2 m^{-2}, across the 12 SAF regions of Table 1. Each value is an average over the whole period of observation. A very tight linear relationship can be seen between the two variables (1 ppm DTE approximately corresponds to 25 g CO_2 m^{-2} over a large range of emission variation (from 18 to 80 g CO_2 m^{-2}). This tight relationship supports the use of DTE as a proxy of fire activity. Regions 3, 5, 4 and 6, as well as the northern part of SAF (ASn) have

ACPD
9, 18621–18657, 2009

the highest values. Region 3 has smaller DTE compared to CO_2 emissions, because of few local extremely high values appearing in GFED data. The atmospheric signature of such intense localized fires is smoothed out by the spatial resolution of the TOVS observations (also, the period of observation is different). Region 7 covering southern Angola and northern Namibia shows lower DTE values than GFEDv2 emissions. This region is dominated by grasslands ecosystems with low fuel loads and emissions. It is also characterized by a relatively large interannual variability (van der Werf et al., 2008; see also next paragraph). The observed bias of DTE is likely to come from the difference in the time periods covered by the two products.

3.1.1 Interannual variability

Figure 4 shows annual means of DTE (Fig. 4a), L3JRC burned area fractions (Fig. 4b), and GFEDv2 emissions (Fig. 4c) for the regions of study, normalized by their means over their respective periods of coverage. Deviations from unity define interannual variability (IAV) in each dataset. Obviously, the IAV of DTE must be taken with care as only 4 years are available, with an El Nino/La Nina couple. Figure 4 shows several interesting features: (1) the low IAV of L3JRC compared to the other two products; (2) the IAV similarities between DTE and GFEDv2, however with exceptions probably due to the too short period covered by DTE. For example, in region 8, the DTE variability entirely depends on the abnormal year 1990 marked by large emissions (Barbosa et al., 1999). In agreement with GFEDv2, the IAV of DTE over forested regions is smaller than over the savannas (see also Ciais et al., 2008). However, because emissions from forested regions are larger in absolute value (see red solid line on Fig. 4c) they still dominate the overall IAV.

The African continent shows a large IAV in carbon balance resulting primarily from climatic perturbations related to El Nino that directly affects the ecosystems productivity and the fire activity (Weber et al., 2009 and references herein, Ciais et al., 2008). Figure 5 compares the 1998–1999 fire emission ratio in GFEDv2, with 1987–1988 ratio in DTE. These pairs of years have the same sequence of an El Niño (1987 and

1998) followed by a La Niña episode (1988 and 1999). A relatively good agreement is seen between DTE and GFEDv2 ratios. For example, one can see values above unity for the eastern regions 4 and 6. This result is coherent with conclusions from Anyamba et al. (2003) or Weber et al. (2009). On the contrary, the ratios disagree for region 8 between DTE and GFEDv2, the reason being an abnormal DTE value for year 1990 and for region 10 characterized by the highest interannual variability in both the DTE and the GFEDv2 data sets (see Fig. 4). Going further into the interpretation of these results is hindered by the fact that fire activity IAV is not always related to climate and vegetation: other factors are equally important because fire has largely become a human-driven phenomenon in the tropics and subtropics (van der Werf et al., 2008; Archibald et al., 2009).

3.2 Seasonal cycles

The seasonal cycles are now compared between DTE and the two other datasets. Figure 6 compares GFEDv2, L3JRC, and DTE seasonal cycles for the 10 regions of SAF and for the two larger regions ASn and ASs. If the overall agreement is relatively satisfactory, this comparison brings into evidence two types of regional behaviour. Over regions 1–5, the seasonal cycles are approximately in phase between DTE and the other two products, yet with a too short fire season in regions 1 and 2. This is due to cloudiness which precludes getting reliable DTE results in May and August. In regions 3 and 5 (although to a lesser extent), the DTE relative seasonal amplitude is smaller than in GFEDv2 and L3JRC which both contain few local extremely high values. For both regions, GFEDv2 (or L3JRC) data larger than the mean $+2.5\,\sigma$ (σ = standard deviation of the distribution) have been rejected because the lower spatial resolution of the DTE approach tends to smooth out such local very intense fires. In regions 6 to 8 and maybe in region 9, the DTE seasonal cycle starts too early and/or too rapidly compared to the other datasets. DTE and L3JRC, which starts one month ahead of GFED, agree better with each other. In region 7 (southern Angola/northern Namibia savannas), DTE shows the largest early bias. Three tentative explanations of this early bias of DTE can

be suggested. First, the DTE observation periods is 10 years apart with GFEDv2, but neither Barbosa et al. (1999) nor Cooke et al. (1996) analyzing coinciding years, did report such an early fire season onset as found in DTE data. Second, advection of fire emissions laden air from northern Africa, a region with active fires in March, could contribute to the observed early DTE signal, given the seasonal winds direction (Edwards et al., 2003; Ryu and Jenkins, 2005); however, this hypothesis would hardly match the diurnal character of the DTE. Third and perhaps more plausible, the early bias of DTE vs. GFEDv2/L3JRC may arise from limits of the burned area detection methods, especially for detecting small burnt scars during the early season. Tansey et al. (2008b) report that the under detection bias of L3JRC product is more significant in areas of shrubs and grasses than over forests. Small but numerous fires are likely to be more frequent during the early fire season. Figure 6 also shows a remarkable agreement for region 10 (Madagascar), where land cover is fairly heterogeneous. For the ASn region, DTE is in phase with L3JRC, but GFEDv2 peaks one month later. For the ASs region, DTE shows a flat maximum from June to September whereas L3JRC peaks in August and GFEDv2 peaks in September. This earlier start of the DTE is consistent with the statement made by Swap et al. (2003) summarizing the main findings of the Southern African Regional Science Initiative SAFARI 2000: "In contrast to the commonly held understanding, the greatest areas burnt were recorded during June and July. The area burned during September comprised only 9% of the fire season total. These results indicate that the fire season peaks earlier than presumed (...) and contradicts the assumptions of several other investigators." An important point is that contamination of the DTE signal by either ozone or dust aerosols is expected to be small at that time of the year. Moreover, a detailed sensitivity analysis by Chédin et al., 2005 also concluded that only high altitude smoke aerosols (above 4 km) with high optical depths (>0.7 at visible wavelengths) could contribute to the enhancement of the DTE signal by ~1 ppm.

In summary, there is a tight relationship between the seasonal cycles of DTE and of fire emission-related products. Despite this, DTE seems to have a systematically

earlier onset than the two other products for regions 6 and 7 (and, to a lesser extent, 8), not yet satisfactorily elucidated.

4 3-D Simulation of the DTE by the general circulation model LMDz

4.1 Model set up over southern Africa

In this section we use 3-D simulations performed with the General Circulation Model LMDz (Hourdin et al., 2006) to assess the credibility of the proposed mechanisms to explain the observed DTE. The GCM includes a parameterization of convective plumes generated by the excess of buoyancy associated with fires, as proposed by Rio et al. (2009). In the so-called "pyro-thermal plume" model, the plume is driven by the heat flux released by the fire and its vertical evolution depends on the area covered by the plume as well as on environmental conditions. The transport of CO_2 emitted by biomass burning over southern Africa in July is simulated using monthly mean CO_2 emissions (see Fig. 7 of Rio et al., 2009) derived from observations gathered during the AMMA field campaign in July 2006 (Liousse et al., 2009). At the beginning of the simulation, the atmosphere is CO_2 free. Within a grid cell, CO_2 daily emission is taken constant throughout the month, with a simple specification of the diurnal cycle: the heat flux and the CO_2 flux released from the surface are assumed to follow a Gaussian time-profile centered on 15:45 LST with a standard deviation of 1 h. The maximum heat flux value is set to 80 kJ m^{-2}. The active burned area for one fire is set to 2 km^2. The simulation allows reproducing CO_2 emitted by fires separately, a signal which can not be distinguished from background CO_2 in the DTE observations.

4.2 Model results for DTE

Rio et al. (2009) show that emitting CO_2 uniformly in the first model layer results in a daily excess of CO_2 of 8 ppm in the two first kilometres. In contrast, activating the

pyro-thermal plume model with emissions injected at the base of the pyro-thermal, leads to a CO_2 excess between evenings and mornings reaching more than 2 ppm in the mid-troposphere when averaged between 5° S and 20° S over the 20 last days of July (Fig. 13 of Rio et al., 2009). The vertical integration of this CO_2 excess leads to a simulated DTE July mean value reaching 1 ppm (Fig. 15 of Rio et al., 2009). This DTE signal cannot be simulated if CO_2 is emitted in the first model layer, where it stays confined in the boundary layer thereafter.

Here, the simulated DTE signal is analysed day by day. Figure 7 shows the simulated integrated concentration of CO_2 from biomass burning as would be seen by TOVS at 07:00 a.m. and 07:00 p.m. for four consecutive days of July. The evening minus morning DTE difference is also shown. If the monthly simulated DTE shows persistent positive values above regions with active fires (Fig. 15 of Rio et al., 2009), it is not always the case when looking at DTE values from day to day. On a daily scale, the modelled DTE signal can be negative over parts of the source region, indicating a higher concentration in the morning than in the evening. Negative daily DTE can also be modelled around the fire source region. However, these daily variations mostly cancel each other out when computing monthly fields. In the simulation, since fire emissions are assumed homogeneous, the modelled DTE variations can only be caused by atmospheric circulation processes. Horizontal winds at 500 hPa averaged over night are drawn upon the modelled CO_2 at 07:00 a.m., and afternoon winds upon modelled CO_2 at 07:00 p.m.

On 18 July (day 1), westerlies from the ocean turn from south-east to north-west when reaching the coast transporting CO_2 from the source region towards the south-east, causing CO_2 accumulation over South Africa and the nearby ocean, leading to a positive DTE there. During 19 July in the afternoon (day 2), winds from the Atlantic ocean penetrate over South Africa, ventilating the CO_2 accumulated south of 15° S, which explains the negative DTE signal over land and the positive signal along the eastern coast south of 15° S that day. On 20 July (day 3), north-westerlies transport CO_2 to the south-east, which explains why the DTE signal is of opposite sign to that of

the day before over ocean.

On 21 July (day 4), the negative DTE signal between 15° S and 25° S over land is due to southerly winds which transport CO_2 present there at 07:00 a.m. to the north during the afternoon. This shows that the variability of DTE from day to day can largely be ascribed to wind fields.

Fires weakly affect the CO_2 seasonal cycle, implying that biomass burning CO_2 does not accumulate locally in the mid-troposphere, but gets advected away from the source region. Figure 8 shows the monthly evolution of CO_2 from biomass burning modelled at 07:00 a.m. and at 07:00 p.m. (left) and of the corresponding DTE signal (right) above 3 points in southern Africa at 20° E–20° S, 20° E–10° S, 20° E–5° S, respectively. At 20° E–10° S, the point located in the center of the fire region, the integrated CO_2 concentration rises rapidly at the beginning of the simulation up to around 2 ppm. On 20 July, CO_2 rises again before stabilizing at 3 ppm. This evolution is associated with DTE which stays positive but varies from day to day, ranging from 0.2 to 1.5 ppm. At the points located at 20° S and 5° S near the boundary of the fire region, the CO_2 signal is much noiser. DTE is either positive or negative depending on the day. Those results show that outside the source region, the daily DTE variations more or less cancel each other on a monthly basis. Over the center of the source region oppositely, DTE is mostly positive, but can still vary by 1 ppm from day to day.

The simulated DTE distribution histogram is presented in Fig. 9 for the two large regions ASn and ASs. These two distributions peak at positive DTE values, but there is a significant tail of negative values. Region ASs has more negative values than ASn and less positive values. Figure 10 shows the distributions of the observed DTE for the same two regions. Simulated and observed distributions both peak at positive DTE values, with ASs having more negative values than ASn and less positive values. Yet, comparing observed and simulated DTE distributions is not straightforward because the simulation assumes the same emissions each day over July while in the real world, fires vary from day to day. In addition, variable background CO_2 and noise from the instrument, retrieval method and from remaining interferences (e.g. undetected thin

ACPD
9, 18621–18657, 2009

clouds) enter into the observed DTE distribution. This difference explains the larger width of the observed distributions. Figures 9 and 10 imply that with the DTE signal resulting from fires is associated a "noise" due to transport (mostly advection). This "noise" possibly causes too small DTE in the morning and too high DTE in the evening. Averaging over a month, the signal sorts out from the noise. Compensation phenomena between abnormally low and abnormally high DTE values approximately maintain the quantitative relationship observed between DTE and emission related products.

4.3 Discussion

The results of the 3-D simulation of DTE essentially confirm the observations:

- the pyro-thermal plume model injects directly a large fraction of fire products in the mid-troposphere well above the planetary boundary layer, where it can be seen by the satellite. Because fire emissions occur mainly during daytime, this produces a 2 ppm amplitude diurnal cycle of CO_2 concentration in the mid-troposphere (Rio et al., 2009), as first seen by Chédin et al. (2005) in the TOVS data;
- the DTE signal contains negative values, particularly south of 15° S outside the fire region. This is likely due to atmospheric circulation patterns over southern Africa in the dry season, characterized by a semi permanent continental gyre throughout the troposphere, particularly south of 10° S, with easterly winds in the tropical band (10° S–20° S), westerly winds in the southern sub-tropical band (20° S–30° S), and meridional winds over the east and west coasts of Africa at around 20° S. On average, this continental gyre prevails approximately half the time during the dry season and is perturbed by westerly waves roughly 30% of the time (Sinha et al., 2003; Jury, 2000). This recirculation pattern opens the possibility for observing morning columns containing more fire emissions than evening columns, i.e. negative DTE. This circulation also can cause afternoon columns to be charged in emissions more than once a day, resulting into higher DTE. As observed and simulated, the DTE is thus not systematically positive but

also takes negative values, even though the monthly mean value remains positive over fire regions.

Two recent studies, one based on observations and one based on simulations confirm our findings. Coheur et al. (2007) using observations from the solar occultation infrared Atmospheric Chemistry Experiment/Fourier Transform Interferometer (ACE/FTS) analyzed a remarkable plume event near the East coast of Tanzania in early October 2005. That plume is characterized by a strong CO concentration enhancement above a background value of about 70–80 ppbv, with a peak value of more than 160 ppbv at about 220 hPa. Their analysis demonstrates that the dominant contribution to the total upper air CO comes from African biomass burning and to a lesser extent from anthropogenic emissions. The plume sampled by the ACE-FTS was young and likely originated from a relatively nearby fire. Freitas et al. (2006, 2007) describe a parameterization to include the vertical transport of hot gases emitted from biomass burning into coarse resolution atmospheric-chemistry-transport models. Their method consists of embedding a 1-D cloud-resolving model in each column of the larger-scale host model. They showed the effect of their "plume rise mechanism" on the vertical distribution of CO. Without plume rise, CO would remain confined into the boundary layer. With it, the boundary layer is polluted by emissions from the smoldering phase whereas a large excess of CO produced during the flaming phase is delivered at about 8 km altitude (Fig. 7 of Freitas et al., 2007). These examples, among others, confirm the mechanism of a rapid uplift and transport of biomass burning emitted CO_2 in the tropical mid-troposphere.

5 Conclusions

The mid-troposphere diurnal CO_2 anomaly between evening and morning (DTE) has been investigated at regional scale over southern Africa with the aim of analyzing its properties as a proxy of fire emission. For that purpose, comparisons have been made between the space and time variability of DTE and fire emission related products

from the Global Fire Emission Database version 2 (GFEDv2) and global burnt areas database of the joint Research Center (L3JRC). Results obtained at seasonal, annual, interannual time-scales for 10 regions in southern Africa with contrasted vegetation cover have brought into evidence striking similarities between DTE and the other two products.

The main difference is a systematically earlier onset in the DTE compared to the two other products for essentially two regions. This earlier DTE bias is not yet elucidated although a tentative explanation has been proposed based on the limits of the burned area detection methods for detecting small burnt scars during the early season. The tight regional correlation between DTE and fire emissions seems to be related to the strong diurnal cycle of fires coupled with fire enhanced convection of CO_2 plumes into the troposphere, seen by the satellite at 19:30 LST, and then transported away from fire regions by large scale winds during night, before the next satellite pass at 07:30 LST.

3-D simulations described by Rio et al. (2009) and performed using the LMDz General Circulation Model including a new pyro-thermal plume model, confirm the DTE magnitude and patterns deduced from the TOVS data:

(1) The pyro-thermal plume model injects a large fraction of fire products into the mid-troposphere, above the planetary boundary layer, where it can be seen by TOVS. Combined with the atmospheric circulation, this vertical transport leads to a daily DTE signal mostly positive over the source region, and either positive or negative outside, so that on a monthly mean basis a DTE signal of ~1 ppm is obtained over regions affected by biomass burning;

(2) The simulated and observed DTE distributions show a small number of negative values occurrences particularly south of 15° S. This is likely due to the mean atmospheric circulation over southern Africa during the dry winter season, characterized by a semi permanent continental gyre prevailing approximately half of the time. This regional recirculation gyre may result in either negative DTE values or in abnormally positive values. Some compensation in the occurrence of

negative and over-positive DTE values can maintain the quantitative relationship observed between DTE and emissions over fire regions.

We conclude from this that DTE observations can be very useful to reconstruct fire emission patterns, in particular before the ATSR, SPOT or MODIS era and can also bring a constraint in the analysis of their present results.

Acknowledgements. This work has been supported in part by the European Community under the contract EVG1-CT-2001-00056 ("COCO") and under the contract FP6-516099 ("GEMS").

The publication of this article is financed by CNRS-INSU.

References

Aardenne van, J. A., Dentener, F. J., Olivier, J. G. J., Klein Goldewijk, C. G. M., and Lelieveld, J.: A 1°×1° resolution data set of historical anthropogenic trace gas emissions for the period 1890–1990, Glob. Change Biol., 15, 909–928, 2001.

Andreae, M. O.: Emissions of trace gases and aerosols from savanna fires, in: Fire in the Southern African Savanna: Ecological and Environmental Perspectives, edited by: van Wilgen, B. W., Andreae M. O., Goldammer J. G., et al., Witwaterstrand University Press, Johannesburg, 161–183, 1996.

Anyamba, A., Justice, C. O., Tucker, C. J., and Mahoney, R.: Seasonal to interannual variability of vegetation and fires at SAFARI 2000 sites inferred from advanced very high resolution radiometer time series data, J. Geophys. Res., 108, 108(D13), 8507, doi:10.1029/2002JD002464, 2003.

Archibald, S., Roy, D. P., van Wilgen, B. W., and Sholes, R. J.: What limits fire? An examination of drivers of burnt area in southern Africa, Glob. Change Biol., 15, 613–630, doi:10.1111/j.1365-2486.2008.01754.x, 2009.

Barbosa, P. M., Stroppiana, D., Grégoire, J. M., and Pereira, J. M. C.: An assessment of vegetation fire in Africa (1981–1991): Burned areas, burned biomass, and atmospheric emissions, Global Biogeochem. Cy., 13, 933–950, 1999.

Bryant, R. G., Bigg, G. R., Mahowald, N. M., Eckardt, F. D., and Ross, S. G.: Dust emission response to climate in southern Africa, J. Geophys. Res., 112, D09207, doi:10.1029/2005JD007025, 2007.

Cahoon, D. R., Stocks, B. J., Levine, J. S., Coter III, W. R., and O'Neill, C. P.: Seasonal distribution of African savanna fires, Nature, 359, 812–815, 1992.

Chédin, A., Serrar, S., Armante, A., Scott, N. A., and Hollingsworth, A.: Signatures of annual and seasonal variations of CO_2 and other greenhouse gases from NOAA/TOVS observations and model simulations, J. Climate, 15, 95–116, 2002.

Chédin, A., Serrar, S., Scott, N. A., Crevoisier, C., and Armante, R.: First global measurement of mid-tropospheric CO_2 from NOAA polar satellites: The tropical zone, J. Geophys. Res., 108, 108(D10), 4301, doi:10.1029/2003JD003439, 2003a.

Chédin, A., Saunders, R., Hollingsworth, A., Scott, N. A., Matricardi, M., Etcheto, J., Clerbaux, C., Armante, R. and Crevoisier, C.: The feasibility of monitoring CO_2 from high resolution infrared sounders, J. Geophys. Res., 108(D2), 4064, doi:10.1029/2001JD001443, 2003b.

Chédin, A., Serrar, S., Scott, N. A., Pierangelo, C., and Ciais, P.: Impact of tropical biomass burning emissions on the diurnal cycle of upper tropospheric CO_2 retrieved from NOAA-10 satellite observations, J. Geophys. Res., 110, D11309, doi:10.1029/2004JD005540, 2005.

Chédin, A., Scott, N. A., Armante, R., Pierangelo, C., Crevoisier, C., Fossé, O., and Ciais, P.: A quantitative link between CO_2 emissions from tropical vegetation fires and the daily tropospheric excess (DTE) of CO_2 seen by NOAA-10 (1987–1991), J. Geophys. Res., 113, D05302, doi:10.1029/2007JD008576, 2008.

Ciais, P., Piao, S.-L., Cadule, P., Friedlingstein, P., and Ch*é*din, A.: Variability and recent trends in the African carbon balance, Biogeosciences Discuss., 5, 3497–3532, 2008, http://www.biogeosciences-discuss.net/5/3497/2008/.

Coheur, P.-F., Herbin, H., Clerbaux, C., Hurtmans, D., Wespes, C., Carleer, M., Turquety, S., Rinsland, C. P., Remedios, J., Hauglustaine, D., Boone, C. D., and Bernath, P. F.: ACE-

FTS observation of a young biomass burning plume: first reported measurements of C_2H_4, C_3H_6O, H_2CO and PAN by infrared occultation from space, Atmos. Chem. Phys., 7, 5437–5446, 2007, http://www.atmos-chem-phys.net/7/5437/2007/.

Cooke, W., Koffi, B., and Grégoire, J. M.: Seasonality of vegetation fires in Africa from remote sensing data and application to a global chemistry model, J. Geophys. Res., 101, 21051–21065, 1996.

Crutzen, P. J. and Zimmermann, P. H.: The changing photochemistry of the troposphere, Tellus, 43AB, 136–151, 1991.

DeFries, R. S., Hansen, M., Townshend, J. R. G., and Sohlberg, R.: Global land cover classifications at 8 km spatial resolution: the use of training data derived from Landsat imagery in decision tree classifiers, Int. J. Remote Sens., 19, 3141–3168, 1998.

Duncan, B. N., Martin, R. V., Staudt, A. C., Yevich, R., and Logan, J. A.: Interannual and seasonal variability of biomass burning emissions constrained by satellite observations, J. Geophys. Res., 108(D2), 4040, doi:10.1029/2002JD002378, 2003.

Freitas, S. R., Longo, K. M., and Andreae, M. O.: Impact of including the plume rise of vegetation fires in numerical simulations of associated atmospheric pollutants, Geophys. Res. Lett., 33, L17808, doi:10.1029/2006GL026608, 2006.

Freitas, S. R., Longo, K. M., Chattfield, R., Latham, D., Silva Dias, M. A., Andreae, M. O., Prins, E., Santos, J. C., Gielow, R., and Carvalho, J. A.: Including the sub-grid scale plume rise of vegetation fires in low resolution atmospheric transport models, Atmos. Chem. Phys., 7, 3385–3398, 2007, http://www.atmos-chem-phys.net/7/3385/2007/.

Giglio, L., Csiszar, I., and Justice, C. O.: Global distribution and seasonality of active fires as observed with the Terra and Aqua Moderate Resolution Imaging Spectroradiometer (MODIS) sensors, J. Geophys. Res., 111, G02016, doi:10.1029/2005JG000142, 2006a.

Giglio, L., van der Werf, G. R., Randerson, J. T., Collatz, G. J., and Kasibhatla, P.: Global estimation of burned area using MODIS active fire observations, Atmos. Chem. Phys., 6, 957–974, 2006b, http://www.atmos-chem-phys.net/6/957/2006/.

Giglio, L.: Characterization of the tropical diurnal fire cycle using VIRS and MODIS observations, Remote Sens. Environ., 108, 407–421, doi:10.1016/j.rse.2006.11.018, 2007.

Hoelzemann, J. J., Schultz, M. G., Brasseur, G. P., Granier, C., and Simon, M.: The Global

Wildland Fire Emission Model GWEM: Evaluating the use of global area burnt satellite data, J. Geophys. Res., 109, D14S04, doi:10.1029/2003JD003666, 2004.
Hoelzemann, J. J.: Global Wildland Fire Emission Modeling for Atmospheric Chemistry Studies, Ph.D. thesis, Max Planck Institute for Meteorology/University of Hamburg, Germany, Reports on Earth System Science, 28/2006, ISSN 1614-1199, 2006.
Hourdin, F., Musat, I., Bony, S., Braconnot, P., Codron, F., Dufresne, J. L., Fairhead, L., Filiberti, M.-A., Friedlingstein, P., Grandpeix, J.-Y., Krinner, G., LeVan, P., Li, Z.-X., and Lott, F.: The LMDz4 general circulation model: climate performance and sensitivity to parametrized physics with emphasis on tropical convection, Clim. Dynam., 27, 787–813, 2006.
Ito, A. and Penner, J. E.: Global estimates of biomass burning emissions based on satellite imagery for the year 2000, J. Geophys. Res., 109, D14S04, doi:10.1029/2003JD004423, 2004.
Jury, M. R.: The dry season climate of tropical southern Africa and implications for pyrogenic emissions, South African J. Sci., 96, 387–390, 2000.
Kasischke, E. S. and Penner, J. E.: Improving global estimates of atmospheric emissions from biomass burning, J. Geophys. Res., 109, D14S01, doi:10.1029/2004JD004972, 2004.
Langenfelds, R. L., Francey, R. J., Pak, B. C., Steele, L. P., Lloyd, J., Trudinger, C. M., and Allison, C. E.: Interannual growth rate variations of atmospheric CO_2 and its $\delta^{13}C$, H_2, CH_4, and CO between 1992 and 1999 linked to biomass burning, Global Biogeochem. Cy., 16(3), 1048, doi:10.1029/2001GB001466, 2002.
Lehsten, V., Tansey, K., Balzter, H., Thonicke, K., Spessa, A., Weber, U., Smith, B., and Arneth, A.: Estimating carbon emissions from African wildfires, Biogeosciences, 6, 349–360, 2009, http://www.biogeosciences.net/6/349/2009/.
Liousse, C., Guillaume, B., Grégoire, J.-M., Mallet, M., Galy, C., Pont, V., Solmon, F., Poirson, A., Rosset, R., Serca, D., Mariscal, A., Dungal, L., Yoboué, V., Bedou, X., Konaré, A., Granier, C., Mieville, A., and van Velthoven, P.: Western African Aerosols Modeling with real time biomass burning emission inventories in the frame of AMMA-IDAF program, Atmos. Chem. Phys., submitted, 2009.
Mayaux, P., Bartholomé, E., Fritz, S., and Belward, A.: A new land-cover map of Africa for the year 2000, J. Biogeogr., 31, 861–877, 2004.
Mouillot, F. and Field, C. D.: Fire history and the global carbon budget: A $1^\circ \times 1^\circ$ fire history reconstruction for the 20th century, Glob. Change Biol., 11, 398–420, 2005.
Palacios-Orueta, A., Chuvieco, E., Parra, A., and Carmona-Moreno, C.: Biomass burning emis-

sions: A review of models using remote-sensing data, Environ. Monit. Assess., 104, 189–209, 2005.
Patra, P. K., Ishizawa, M., and Maksyutov, S.: Role of biomass burning and biomass anomalies for land-atmosphere carbon fluxes based on inverse modeling of atmospheric CO_2, Global Biogeochem. Cy., 19, GB3005, doi:10.1029/2004GB002258, 2005.
Potter, C. S., Randerson, J. T., Field, C. B., Matson, P. A., Vitousek, P. M., Mooney, H. A., and Klooster, S. A.: Terrestrial ecosystem production: A process-oriented model based on global satellite and surface data, Global Biogeochem. Cy., 7, 811–842, doi:10.1029/93GB02725, 1993.
Randerson, J. T., Thompson, M. V., Conway, T. J., Field, C. B., and Fung, I. Y.: Substrate limitations for heterotrophs: Implications formodels that estimate the seasonal cycle of atmospheric CO_2, Global Biogeochem. Cy., 10(4), 585–602, doi:10.1029/96GB01981, 1996.
Randerson, J. T., van der Werf, G. R., Collatz, G. J., Giglio, L., Still, C. J., Kasibhatla, P., Miller, J. B., White, J. W. C., DeFries, R. S., and Kasischke, E. S.: Fire emissions from C_3 and C_4 vegetation and their influence on interannual variability of atmospheric CO_2 and $\delta^{13}CO_2$, Global Biogeochem. Cy., 19, GB2019, doi:10.1029/2004GB002366, 2005.
Randerson, J. T., van der Werf, G. R., Giglio, L., Collatz, G. J., and Kasibhatla, P. S.: Global Fire Emissions Database, Version 2 (GFEDv2), available on-line (http://daac.ornl.gov/) from Oak Ridge National Laboratory Distributed Active Archive Center, Oak Ridge, Tennessee, USA, 2006.
Rio, C., Hourdin, F., and Chédin, A.: Numerical simulation of tropospheric injection of biomass burning products by pyro-thermal plumes, Atmos. Chem. Phys. Discuss, accepted, 2009.
Rumelhart, D. E., Hinton, G. E., and Williams, R. J.: Learning internal representations by error propagation, in: Parallel Distributed Processing: Explorations in the Macrostructure of Cognition, edited by: Rumelhart, D. E. and McClelland, J. L., MIT Press, Cambridge, 318–362, 1986.
Ryu, J.-H. and Jenkins, G. S.: Lightning-tropospheric ozone connections: EOF analysis of TCO and lightning data, Atmos. Environ., 39, 5799–5805, 2005.
Schultz, M. G.: On the use of ATSR fire count data to estimate the seasonal and interannual variability of vegetation fire emissions, Atmos. Chem. Phys., 2, 387–395, 2002, http://www.atmos-chem-phys.net/2/387/2002/.
Schultz, M. G., Wooster, M., Boucher, O., Doutriaux-Boucher, M., Granier, C., Heil, A., Hollingsworth, A., Kaiser, J. W., Kasilowski, T., Morcrette, J.-J., Roberts, G., Simmons, A.,

and van der Werf, G. R.: Evaluation of a fire radiative power product derived from Meteosat 8/9 and identification of operational use, Final Report, EUMETSAT contract EUM/CO/06/4600000277/YG, 139 pp., 2008.
Sinha, P., Hobbs, P. V., Yokelson, R. J., Blake, D. R., Gao, S., and Kirchstetter, T. W.: Distributions of trace gases and aerosols during the dry biomass burning season in southern Africa, J. Geophys. Res., 108(D17), 4536, doi:10.1029/2003JD003691, 2003.
Smith, W. L., Woolf, H. M., Hayden, C. M., Wark, D. Q., and McMillin, L. M.: The TIROS-N Operational Vertical Sounder, B. Am. Meteorol. Soc., 60, 1177–1187, 1979.
Swap, R. J., Annegarn, H, J., Suttles, J. T., King, M. D., Platnick, S., Privette, J. L., and Scholes, R. J.: Africa burning: A thematic analysis of the Southern African Regional Science Initiative (SAFARI 2000), J. Geophys. Res., D13, 8465, doi:10.1029/2003JD003747, 2003.
Tansey, K., Grégoire, J.-M., Defourny, P., Leigh, R., Pekel, J.-F., van Bogaert, E., and Bartholomé, E.: A new, global, multi-annual (2000–2007) burnt area product at 1 km resolution, Geophys. Res. Lett., 35, L01401, doi:10.1029/2007GL031567, 2008a.
Tansey, K., Beston, J., Hoscilo, A., Page, S. E., and Paredes Hernandez, C. U.: Relationship between MODIS fire hot spot count and burned area in a degraded tropical peat swamp forest in Central Kalimantan, Indonesia, J. Geophys. Res., 113, D23112, doi:10.1029/2008JD010717, 2008b.
van der Werf, G. R., Randerson, J. T., Collatz, G. J., and Giglio, L.: Carbon emissions from fires in tropical and subtropical ecosystems, Glob. Change Biol., 9, 547–562, 2003.
van der Werf, G. R., Randerson, J. T., Collatz, G. J., Giglio, L., Kasibhatla, P. S., Arellano Jr., A. F., Olsen, S. C., and Kasischke, E. S.: Continental partitioning of fire emissions during the 1997 to 2001 El Nino/La Nina period, Science, 303, 73–76, 2004.
van der Werf, G. R., Randerson, J. T., Giglio, L., Collatz, G. J., Kasibhatla, P. S., and Arellano Jr., A. F.: Interannual variability in global biomass burning emissions from 1997 to 2004, Atmos. Chem. Phys., 6, 3423–3441, 2006, http://www.atmos-chem-phys.net/6/3423/2006/.
van der Werf, G. R., Randerson, J. T., Giglio, L., Gobron, N., and Dolman, A. J.: Climate controls on the variability of fires in the tropics and subtropics, Glob. Biogeochem. Cy., 22, GB3028, doi:10.1029/2007GB003122, 2008.
Weber, U., Jung, M., Reichstein, M., Beer, C., Braakhekke, M. C., Lehsten, V., Ghent, D., Kaduk, J., Viovy, N., Ciais, P., Gobron, N., and Rödenbeck, C.: The interannual variability of Africa's ecosystem productivity: a multi-model analysis, Biogeosciences, 6, 285–295, 2009,

http://www.biogeosciences.net/6/285/2009/.
Wittenberg, U., Heimann, M., Esser, G., David McGuire, A., and Sauf, W.: On the influence of biomass burning on the seasonal CO_2 signal as observed at monitoring stations, Glob. Biogeochem. Cy., 12, 531–544, 1998.
Ziemke, J. R., Chandra, S., Duncan, B. N., Froidevaux, L., Bhartia, P. K., Levelt, P. F., and Waters, J. W.: Tropospheric ozone determined from Aura OMI and MLS: Evaluation of measurements and comparison with the Global Modeling Initiative's Chemical Transport Model, J. Geophys. Res., 111, D19303, doi:10.1029/2006JD007089, 2006.

Table 1. Limits in latitude and longitude of the 10 regions used in this study (adapted from Hoelzemann et al., 2006). The two regions ASn and ASs integrate the northern and the southern parts of southern Africa, respectively.

Region code	Latitude min	Latitude max	Longitude min	Longitude max
H1	−6	0	8	28
H2	−6	0	28	43
H3	−10	−6	10	28
H4	−10	−6	28	40
H5	−14	−10	10	28
H6	−14	−10	28	43
H7	−25	−14	10	20
H8	−25	−14	20	28
H9	−25	−14	28	40
H10	−25	−12	42	50
ASs	−25	−15	8	43
ASn	−15	0	8	43

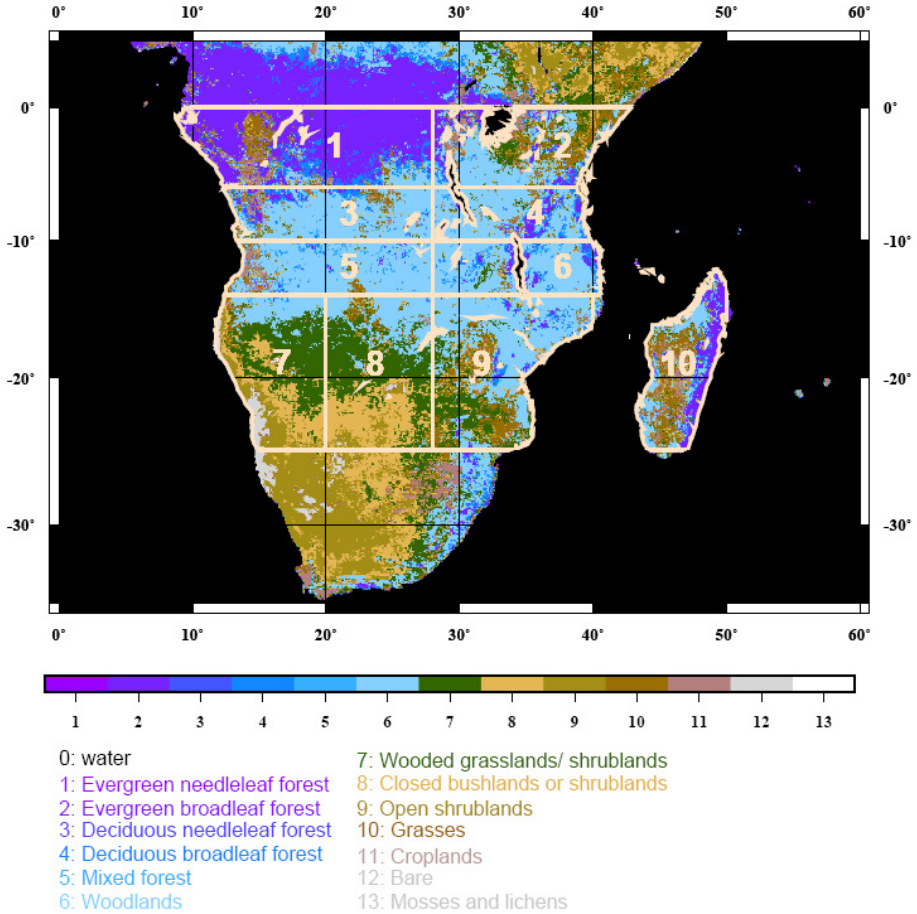

Fig. 1. The 10 regions of the study adapted from Hoelzemann (2006). Note the change in the southern-most limit: 25° S here, instead of 34° S in the above reference. Vegetation map is from DeFries et al. (1998).

ACPD

9, 18621–18657, 2009

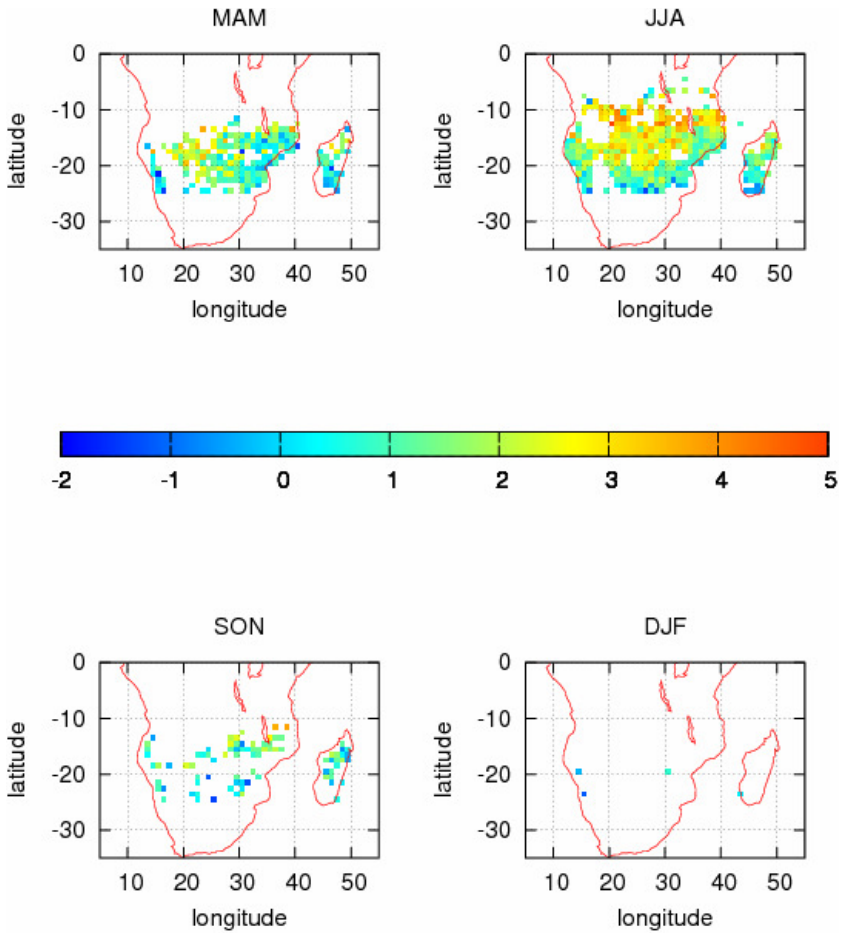

Fig. 2. Four-year averaged seasonal maps of the DTE.

ACPD
9, 18621–18657, 2009

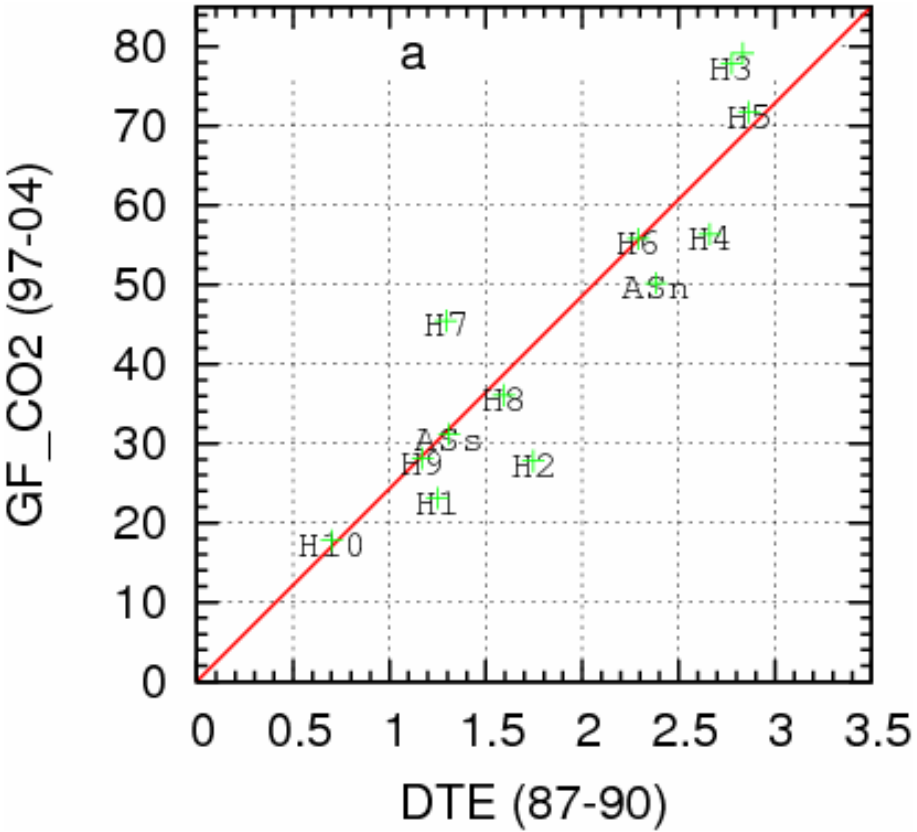

Fig. 3. GFEDv2 CO_2 annual mean emissions (in $g\,CO_2\,m^{-2}$) averaged over the period 1997–2004 (van der Werf et al., 2006) versus annual mean DTE (in ppm) averaged over the period 1987–1990 for the 10 regions of the study and the 2 integrated ASn and ASs regions.

ACPD
9, 18621–18657, 2009

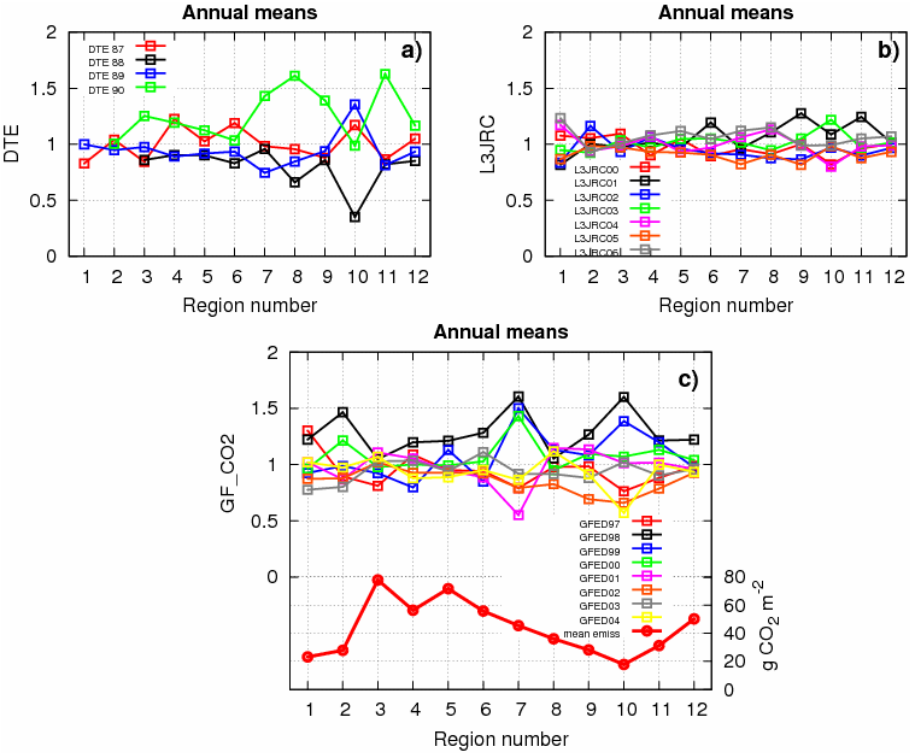

Fig. 4. Annual means of DTE (**a**), L3JRC burned fractions (**b**), and GFED CO_2 emissions (**c**) for the regions of study, normalized by their mean over their respective time periods: (1987–1990), (1997–2004), and (2000–2007). Missing data in Fig. 4a are due to too small numbers of items available. The red solid line in Fig. 4c shows the GFED CO_2 emissions (in g CO_2 m^{-2}) averaged over the period 1997–2004.

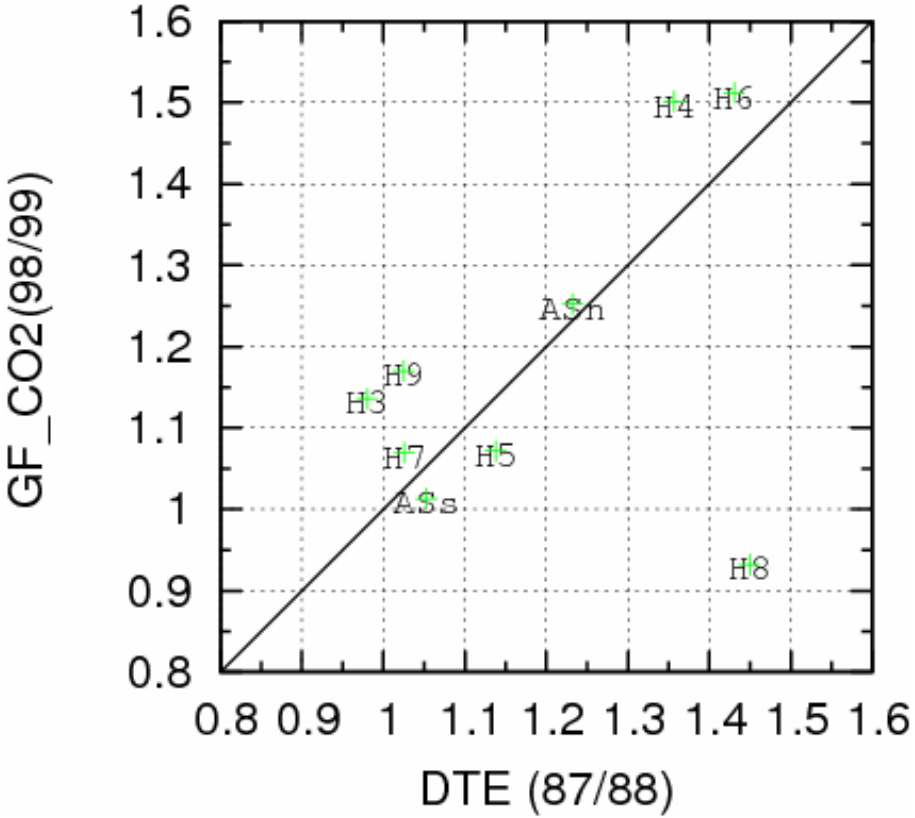

Fig. 5. Ratio of emissions in 1998 to the emissions in 1999 in GFEDv2 vs. the ratio of DTE in 1987–1988. The selected pairs of years are both composed of an El Niño year (1987 and 1998) and a La Niña year (1988 and 1999). Missing data are due to too small number of items available (regions 1 and 2) or to a result out of the graph (region 10; see text).

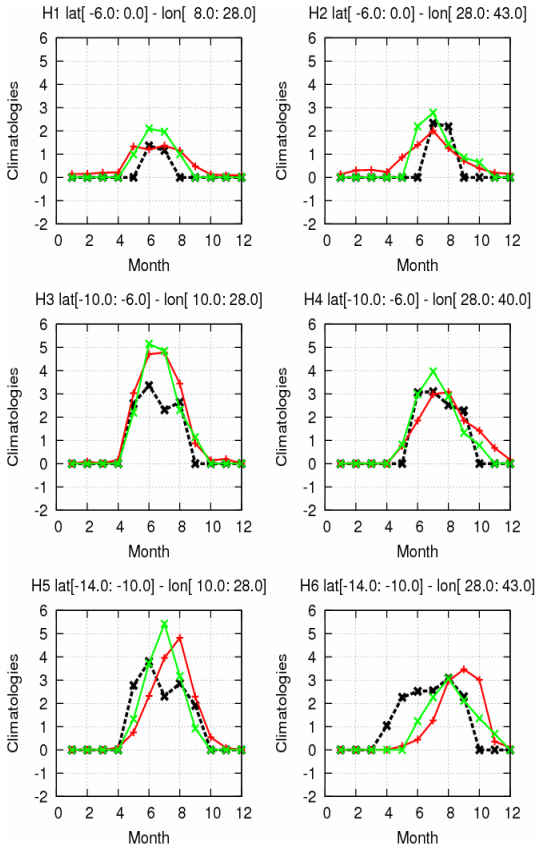

Fig. 6. Seasonal cycles of: DTE (in ppm, averaged over 1987–1990, dashed black); GFEDv2 CO_2 emission (in g CO_2 m^{-2}, averaged over 1997–2004, red); L3JRC burned fraction (averaged over 2000–2007, green). Both GFED and L3JRC values have been scaled to fit the DTE value range.

ACPD
9, 18621–18657, 2009

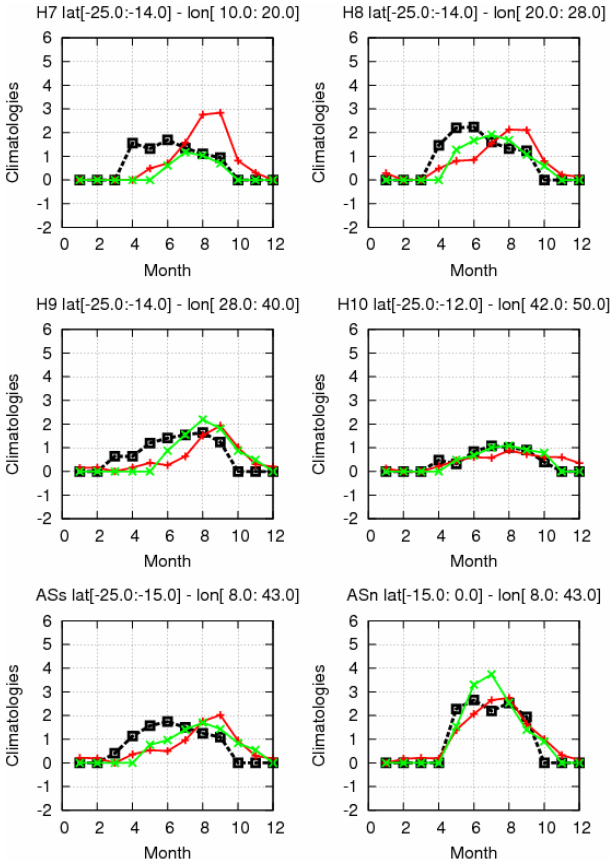

Fig. 6. Continued.

ACPD
9, 18621–18657, 2009

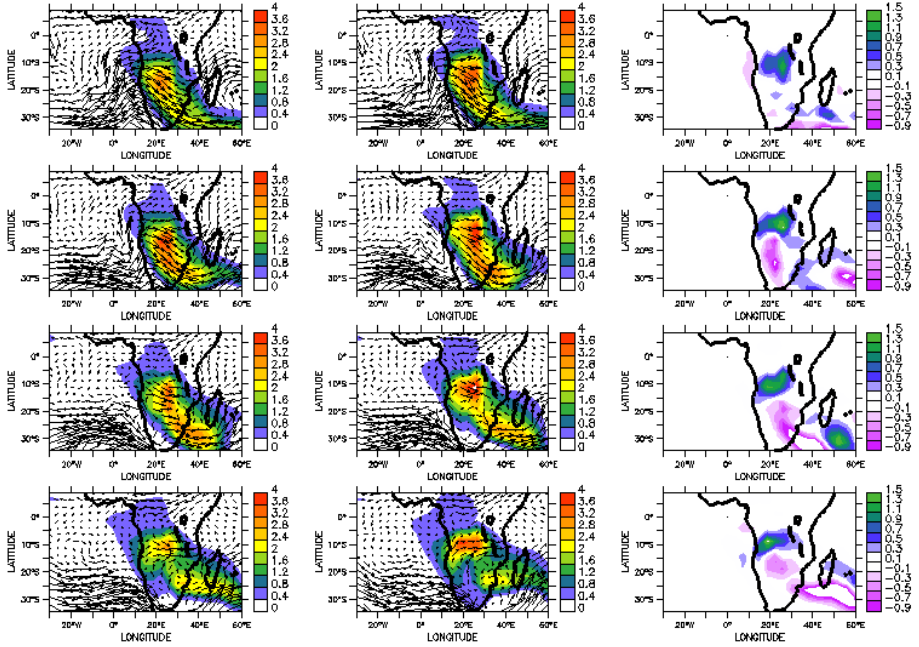

Fig. 7. Simulated integrated CO_2 concentration from biomass burning which would be retrieved from satellite at 07:00 a.m. (left), and 07:00 p.m. (middle) and the difference between the concentration at 07:00 p.m. and the one at 07:00 a.m. (right), on (from top to bottom) the 18–21 July.

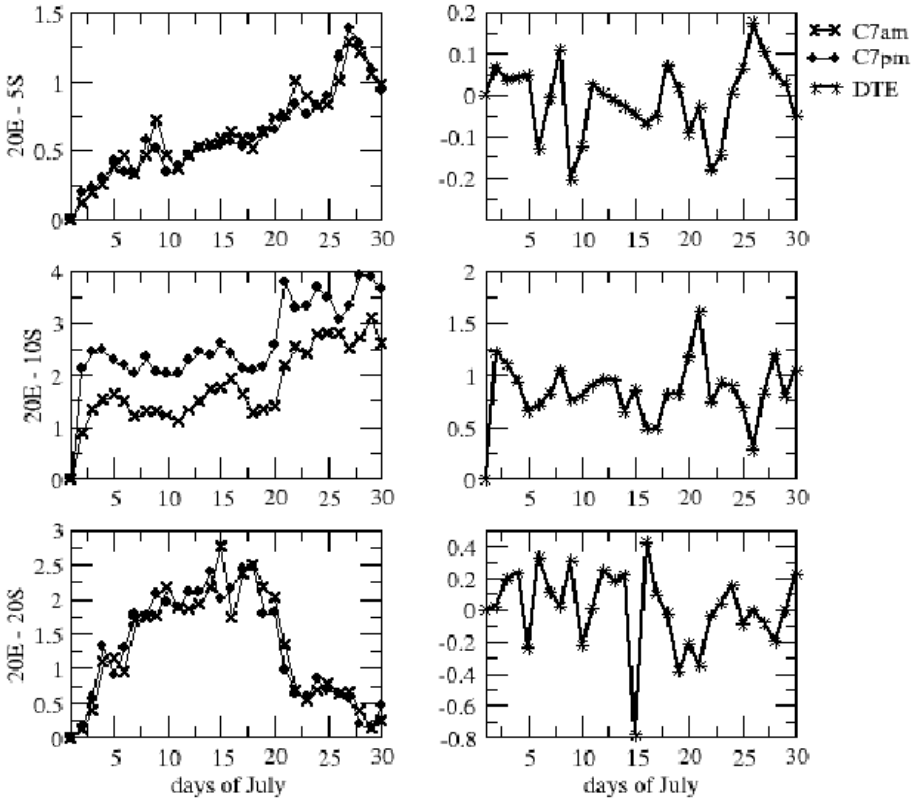

Fig. 8. Monthly evolution of the simulated concentration as seen by the satellite at 07:00 a.m. and 07:00 p.m. (left) and of the simulated DTE signal (right) at three different locations over southern Africa, north of the source region (20° E–5° S), in the middle of the source region (20° E–10° S) and south of the source region (20° E–20° S), from top to bottom.

ACPD
9, 18621–18657, 2009

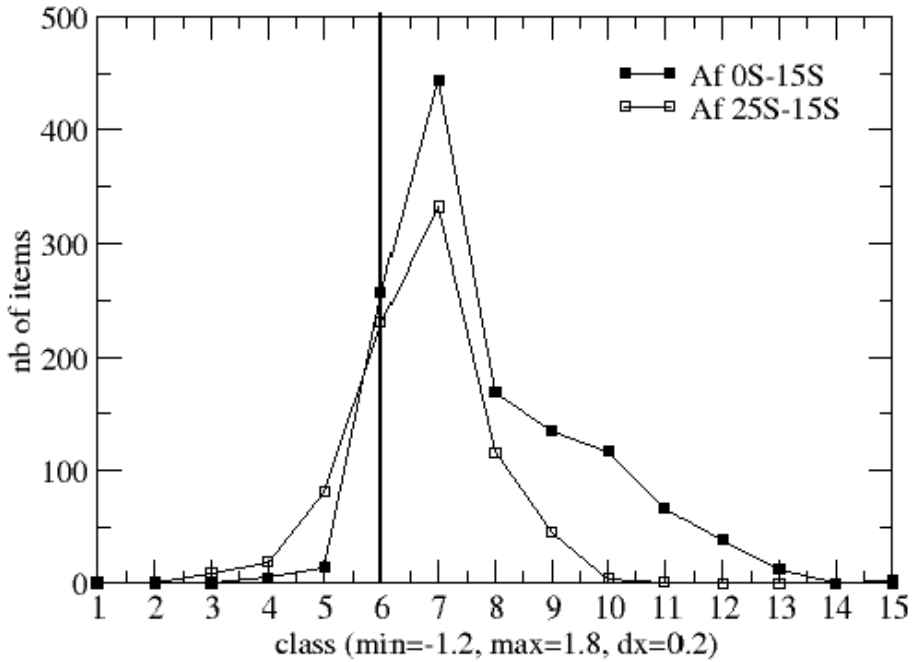

Fig. 9. Distribution of the modelled DTE signal of July for regions Afn and Afs; class 6 is for DTE ranging from −0.2 to 0, class 7 from 0 to 0.2, etc.

ACPD
9, 18621–18657, 2009

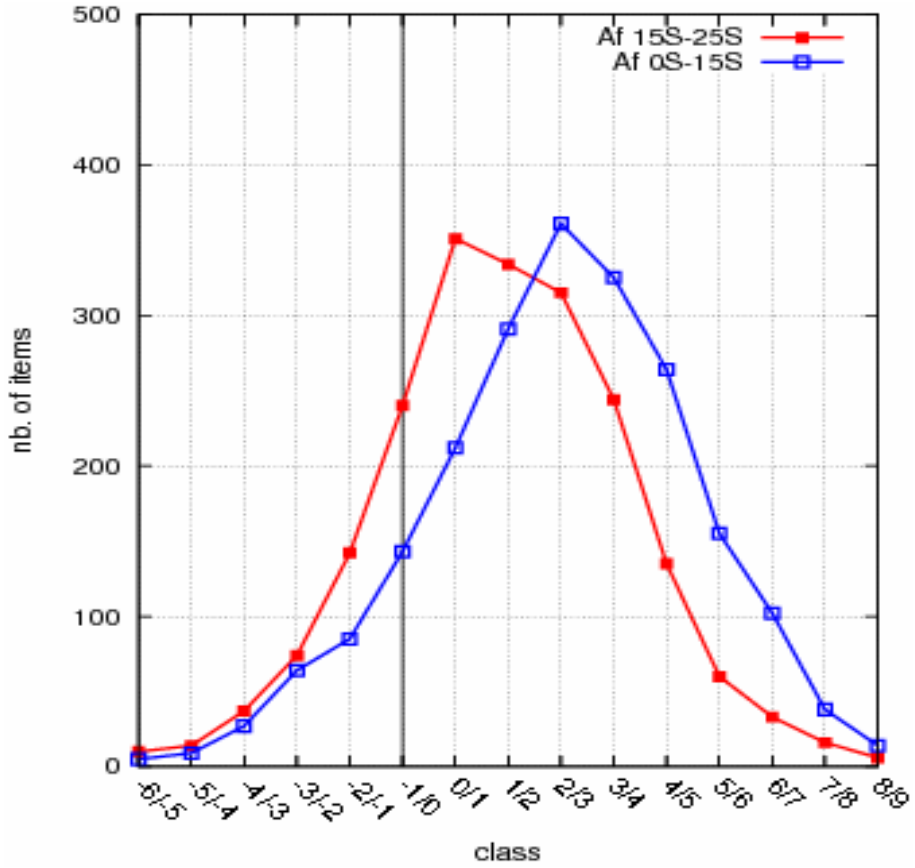

Fig. 10. Histograms of the observed DTE for the season June, July, and August of the period 1987–1990; class "−1/0" is for DTE values (in ppm) ranging from −1 to 0.